

## **Direct and indirect photodegradation of atrazine and S-metolachlor in agriculturally impacted surface water and associated C and N isotope fractionation†**

Guillaume Drouin,<sup>‡a</sup> Boris Droz,<sup>‡\*a</sup> Frank Leresche,<sup>b</sup> Sylvain Payraudeau,<sup>a</sup> Jérémy Masbou<sup>a</sup> and Gwenaël Imfeld<sup>\*a</sup>

*<sup>a.</sup> Institut Terre et Environnement de Strasbourg (ITES), Université de Strasbourg/EOST/ENGEEES, CNRS UMR 7063, 5 rue Descartes, Strasbourg F-67084, France.*

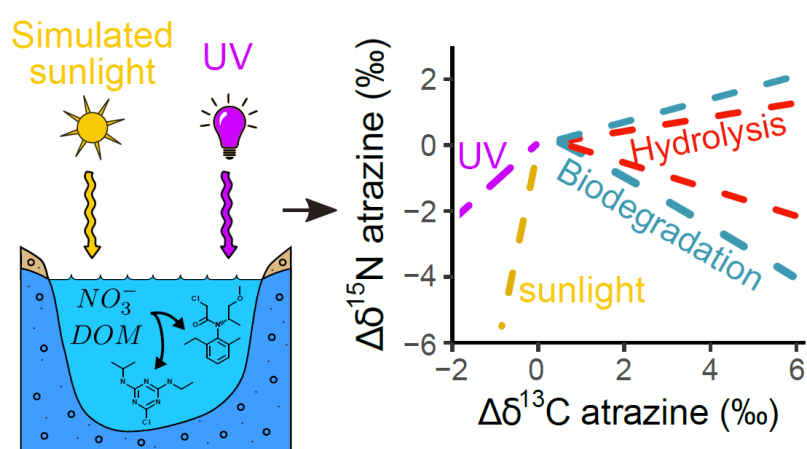
*<sup>b.</sup> Department of Civil, Environmental, and Architectural Engineering, Environmental Engineering Program, University of Colorado Boulder, Colorado 80309, United States.*

† Electronic Supplementary Information (ESI) available: Complete list of chemicals, description of the photobleaching control and, PNA/Pyr actinometer system, characterization of the photoreactor system, details on the analytical methods for pesticide quantification, CSIA measurement and TPs elucidation, calculation of short-lived reactive intermediates, steady state concentrations, of light absorption rates and screening factors and raw results.

‡ These authors contributed equally to the publication.

## Abstract

Knowledge of direct and indirect photodegradation of pesticides and associated isotope fractionation can help to assess pesticide degradation in surface waters. Here, we investigated carbon (C) and nitrogen (N) isotope fractionation during direct and indirect photodegradation of the herbicides atrazine and *S*-metolachlor in synthetic water, mimicking agriculturally impacted surface waters containing nitrates ( $20 \text{ mg L}^{-1}$ ) and dissolved organic matter (DOM,  $5.4 \text{ mg}_C \text{ L}^{-1}$ ). Atrazine and *S*-metolachlor were quickly photodegraded by both direct and indirect pathways (half-lives  $<5$  and  $<7$  days, respectively). DOM slowed down photodegradation while nitrates increased degradation rates. The analysis of transformation products showed that oxidation mediated by hydroxyl radicals ( $\text{HO}\cdot$ ) predominates during indirect photodegradation. UV light (254 nm) caused significant C and N isotope fractionation, yielding isotope enrichment factors  $\epsilon_C = 2.7 \pm 0.3$  and  $0.8 \pm 0.1\text{‰}$ , and  $\epsilon_N = 2.4 \pm 0.3$  and  $-2.6 \pm 0.7\text{‰}$  for atrazine and *S*-metolachlor, respectively. In contrast, photodegradation under simulated sunlight led to negligible C and slight N isotope fractionation, indicating the influence of the radiation wavelength on the direct photodegradation-induced isotope fractionation. Altogether, this study highlights the relevance of using simulated sunlight to evaluate photodegradation pathways in the environment and the potential of CSIA to distinguish photodegradation from other dissipation pathways in surface waters.



TOC FIGURE

## 1 **Environmental significance**

2 Ubiquitous pesticide contamination of surface waters is a crucial environmental issue. Little is  
3 known about pesticide photodegradation in agriculturally impacted surface waters, where  
4 nitrates and dissolved organic matter (DOM) co-occur. This study addresses this bottleneck by  
5 examining pesticide photodegradation in agriculturally impacted surface waters with nitrates and  
6 DOM. It provides reference isotope enrichment factors for direct and indirect photodegradation  
7 of atrazine and *S*-metolachlor in surface waters. We show that compound-specific isotope analysis  
8 (CSIA) can help to differentiate photodegradation from other dissipation pathways in surface  
9 waters. Our results also advocate for more systematic use of simulated sunlight when  
10 characterizing photodegradation mechanisms in laboratory experiments.

## 11 **Introduction**

12 The ever-increasing use of pesticides, mainly for agricultural purposes, has led to ubiquitous  
13 contamination of surface waters,<sup>1</sup> which may affect environmental biodiversity and human  
14 health.<sup>2</sup> Thus, understanding pesticide transformation in surface waters is crucial to achieve  
15 accurate persistence predictions, anticipate the formation of transformation products (TPs) and  
16 help to mitigate detrimental effects of further pollution. While biodegradation is a major pathway  
17 of pesticide degradation in the environment, photodegradation also plays a prominent role in  
18 surface waters.<sup>3</sup> Pesticide photodegradation is compound- and condition-specific, which often  
19 limits the interpretation of photodegradation kinetics and pathways in various types of surface  
20 waters.<sup>4, 5</sup> In particular, the influence of the hydrochemical composition, the nature of dissolved

21 organic matter (DOM) as well as the light spectrum on pesticide photodegradation remains poorly  
22 understood.<sup>6,7</sup>

23 Pesticides undergo photodegradation by direct and indirect pathways. During direct  
24 photodegradation, pesticide molecules absorb light, resulting in bond cleavage. Indirect  
25 photodegradation involves reactions with short-lived reactive intermediates, such as hydroxyl  
26 radical (HO•) or DOM excited triplet states (<sup>3</sup>DOM\*<sup>8</sup>). Nitrate photolysis produces HO• that can  
27 react with pesticides in surface waters, even at nitrate concentrations as low as 0.02 mg L<sup>-1</sup>.<sup>5</sup> DOM  
28 has inhibitory and/or photosensitizing effects, depending on its concentration and composition.<sup>9</sup>  
29 On the one hand, DOM absorbs light, reducing direct photodegradation of pesticides and HO•  
30 generation from nitrate photolysis. On the other hand, upon light absorption, DOM generates  
31 <sup>3</sup>DOM\* which is the precursor of singlet molecular oxygen (<sup>1</sup>O<sub>2</sub>) in surface waters. Both <sup>3</sup>DOM\* and  
32 <sup>1</sup>O<sub>2</sub> can react with pesticides. DOM is also a major sink of HO• in surface waters, reducing HO•  
33 reactions with pesticides. DOM can also reduce pesticide oxidation intermediates back to the  
34 parent compounds, and limit pesticide photodegradation.<sup>10</sup> The effect of DOM on pesticide  
35 photodegradation is, however, compound-specific and mostly involves unknown mechanisms.<sup>11</sup>  
36 While the combined effects of nitrates and DOM on pesticide photodegradation is relevant for  
37 surface waters in agricultural areas, few studies on the topic have been conducted.<sup>4, 12</sup>

38 Compound-specific isotope analysis (CSIA) has been used in diverse environmental compartments  
39 to investigate micropollutant degradation, including pesticides and pharmaceuticals.<sup>13</sup> Pollutant  
40 molecules with different ratios of light over heavy stable isotopes are degraded at slightly different  
41 rates. This results in a kinetic isotope effect (KIE) quantifiable by CSIA.<sup>14</sup> In contrast, dilution, such  
42 as transport or sorption, generally does not alter significantly stable isotope ratios (e.g., <sup>2</sup>H/<sup>1</sup>H,  
43 <sup>13</sup>C/<sup>12</sup>C, and <sup>15</sup>N/<sup>14</sup>N) within pollutant molecules.<sup>15</sup> The KIE reflects the rate-limiting step of the

44 involved pathway. Each degradation pathway displays a specific isotope fractionation pattern.  
45 This enables to differentiate the contribution of co-occurring degradation pathways in the  
46 environment. For example, CSIA was used to distinguish direct photodegradation from other  
47 degradation pathways, including biodegradation, abiotic oxidation and dilution, affecting the  
48 dissipation of diclofenac in riverine systems.<sup>15</sup> Although CSIA has been applied to characterize  
49 pesticide degradation in the environment,<sup>13</sup> little is known about stable isotope fractionation of  
50 pesticides during direct and indirect photodegradation in surface waters.

51 To the best of our knowledge, only Hartenbach et al.<sup>17</sup> have evaluated isotope fractionation for  
52 direct and indirect photodegradation of atrazine under specific conditions of irradiation and water  
53 chemistry. However, isotope fractionation may depend on the irradiation source and the DOM  
54 nature. Negligible carbon (C) isotope fractionation of the antibiotic sulfamethoxazole was  
55 observed in experiments with UVC light, while significant isotope enrichment factor ( $\epsilon_C = -4.8 \pm$   
56  $0.1\text{‰}$ ) was observed when UVB and UVA prevailed.<sup>18</sup> Slight C isotope enrichment factor ( $\epsilon_C = -$   
57  $0.7 \pm 0.2\text{‰}$ ) was also observed during direct photodegradation of diclofenac under sunlight.<sup>16</sup>  
58 Differences in C and nitrogen (N) isotope fractionation patterns suggest distinct pathways  
59 associated with photodegradation of the nitrile herbicide bromoxynil when irradiated either with  
60 a UV lamp or exposed to sunlight under environmental conditions.<sup>19</sup> Isotope fractionation may  
61 also depend on the nature of DOM and its propensity to favor HO• and <sup>3</sup>DOM\* short-lived reactive  
62 intermediates oxidation. This has been observed for both methyl and ethyl *tert*-butyl ether.<sup>20</sup>  
63 Although these results emphasize the potential of CSIA to evaluate photodegradation in  
64 laboratories and in natural systems, reference isotope enrichment factor to characterize pesticide  
65 photodegradation in agriculturally impacted surface waters are currently missing.

66 In this context, the purpose of this study was to examine typical patterns of photodegradation and  
67 associated isotope fractionation for atrazine and *S*-metolachlor in agriculturally impacted surface  
68 waters. We irradiated atrazine and *S*-metolachlor with simulated sunlight ( $\lambda$  from 270 to 720 nm)  
69 under hydrochemical conditions representative of surface waters in agricultural settings (DOM =  
70  $5.4 \text{ mg}_C \text{ L}^{-1}$ ;  $\text{NO}_3^- = 20 \text{ mg L}^{-1}$ ). We hypothesized that the hydrochemical composition of surface  
71 waters differently affects direct and indirect pathways of pesticide photodegradation and  
72 associated isotope fractionation. In particular, irradiation of nitrates and DOM may lead to the  
73 formation of short-lived reactive intermediates controlling underlying photodegradation  
74 pathways. Thus, direct and indirect photodegradation of pesticides were tested separately and  
75 concomitantly, in the presence of nitrates and/or DOM. C and N isotope enrichment factors were  
76 derived for direct and indirect photodegradation of atrazine and *S*-metolachlor. Complementary  
77 experiments were conducted under UV light ( $\lambda = 254 \text{ nm}$ ) to evaluate the effect of the irradiation  
78 wavelengths on C and N isotope fractionation during pesticide photodegradation.

79

## 80 **Materials and methods**

### 81 **Chemicals and preparation of solutions**

82 All chemicals were at least HPLC grade (>97%) (more detail in ESI<sup>†</sup>). Atrazine and *S*-metolachlor  
83 (Pestanal, >99.9%) stock solutions were individually prepared at  $5 \text{ g L}^{-1}$  in dichloromethane (DCM)  
84 and aliquots were stored at  $-20^\circ\text{C}$  in brown glass vials. Before irradiation, pesticide stock solutions  
85 were spiked and stirred for one hour, until complete DCM volatilization. Suwannee River Fulvic  
86 Acid (SRFA - 2S101F) was obtained from the International Humic Substances Society (IHSS) and  
87 selected as a source of DOM representative of headwater rivers.<sup>20</sup> Stock solutions of SRFA were  
88 prepared at a concentration of  $50 \text{ mg L}^{-1}$  by dissolving 10 mg of SRFA in 100 mL of ultrapure water

89 (UW; Resistivity >15M $\Omega$ , dissolved organic matter (DOM; <0.2 mg C L<sup>-1</sup>), followed by 15 min  
90 sonication (Branson 5510, 40 kHz). The solutions were filtered through sterile 0.22  $\mu$ m pore  
91 diameter cellulose acetate membranes and stored at 4°C in brown glass vials. The synthetic  
92 surface water was prepared to target the ionic composition of typical soft surface waters.<sup>21</sup>

93

#### 94 **Photodegradation experiment**

95 Atrazine and *S*-metolachlor were selected as representatives of widely used and ubiquitously  
96 detected triazine and chloroacetanilide pesticides,<sup>1</sup> and based on expected degradation kinetics.  
97 Direct photolysis experiments (DIR) were carried out at room temperature (20  $\pm$  5 °C)  
98 independently for atrazine and *S*-metolachlor in UW with a 50 mM phosphate buffer  
99 (KH<sub>2</sub>PO<sub>4</sub>/Na<sub>2</sub>HPO<sub>4</sub>) at *pH* = 7.9  $\pm$  0.2, as it has no significant effects on photodegradation rates and  
100 isotope fractionation.<sup>22</sup> The effect of nitrates (NIT) on pesticide photodegradation was  
101 investigated in buffered synthetic water by adding 331  $\pm$  2  $\mu$ M of sodium nitrate salts (NO<sub>3</sub><sup>-</sup> = 20  
102 mg L<sup>-1</sup>), representative of agriculturally impacted surface waters in Europe.<sup>23</sup> The effect of DOM  
103 (SRFA) was studied by adding 5.4  $\pm$  0.2 mg<sub>C</sub> L<sup>-1</sup> of SRFA, considered as a representative  
104 concentration of rivers worldwide.<sup>24</sup> The combined effect of nitrates and DOM (TOT) was  
105 investigated in synthetic water, spiked with sodium nitrates, SRFA and atrazine (5  $\mu$ M) or *S*-  
106 metolachlor (3  $\mu$ M) (Table S1 in the ESI<sup>†</sup>).

107 The DIR, NIT, SRFA, and TOT experiments were conducted in a 500 mL quartz tube ( $\varnothing$  = 5 cm)  
108 irradiated until the non-degraded fraction ( $C_t/C_0$ ) was below 10% for atrazine and *S*-metolachlor,  
109 corresponding to an irradiation duration from 7 to 600 hours. Aliquots from 15 to 200 mL were  
110 sequentially collected during the experiments. Although the light path changed over repetitive  
111 samplings and affected the screening factor (eq. S9 in the ESI<sup>†</sup>), it did not affect kinetics rates and

112 the contribution of the different processes. Insignificant degradation (<5%) in sterile and dark  
113 controls for all experimental conditions indicated insignificant hydrolysis and biodegradation  
114 during the photodegradation experiments. Photo-bleaching of DOM by HO• only slightly  
115 decreased the initial DOM content (<18%) after more than 310 h of irradiation (Fig. S1 in the ESI†).  
116 Irradiation conditions in the experiments with DOM were thus assumed constant.

117 DIR, NIT, SRFA, and TOT irradiations were carried out under simulated sunlight with a stand-alone  
118 lighting system (Lambda LS, Sutter Instrument) fitted with a 300 W xenon (Xe) arc lamp (P/N  
119 PE300BUV, Cemax). A liquid optical fiber transmitted the light to a quartz tube covered with an  
120 aluminium foil with a cut-off of UV radiations below  $\lambda = 270\text{nm}$ . The light spectrum (Fig. S4 in the  
121 ESI†) obtained through the quartz tube, characterized with a calibrated spectroradiometer ILT  
122 900C (International Light), was in the range 270 to 720 nm. The mean photon fluence rate was  
123 estimated to be  $7 \mu\text{E m}^{-2} \text{s}^{-1}$  in the 290 to 400 nm range using a *p*-nitroanisole (PNA; 30  
124  $\mu\text{M}$ )/pyridine (10 mM) actinometer system prepared as previously described.<sup>25</sup> Up to date values  
125 of wavelength-independent quantum yields for PNA,  $\phi_{PNA} = 3.19 \times 10^{-3} \text{ mol E}^{-1}$  were used  
126 (detailed in ESI†).<sup>26</sup> Due to long irradiation times, fluctuations of light intensity were monitored  
127 for the ranges of UVA ( $320 < \lambda < 400 \text{ nm}$ ), UVB ( $280 < \lambda < 320 \text{ nm}$ ) and visible light (VIS,  $360 < \lambda < 830$   
128 nm) using a calibrated SOLAR light PMA2200 radiometer. The Xe arc lamps were systematically  
129 replaced when the total light intensity dropped or whenever shift in the UVA/UVB/VIS ratios  
130 exceeded 5% of the original value (Table S2 in the ESI†).

131 Additional direct photolysis experiments were carried out at 254 nm (DIR254) to investigate the  
132 effect of the irradiation wavelength on direct photodegradation. The photodegradation of  
133 pesticides was examined using a light-proof box (P/N 701 435, Jeulin) with black material equipped  
134 with a low-pressure mercury lamp (LP Hg; P/N TUV G6T5, Phillips – nominal power 6W) lamp

135 providing a major band at 254 nm with 22% of secondary bands (light band intensities are  
136 provided in Table S3 in the ESI†). 50 mL beakers (int.  $\varnothing = 37$  mm) in borosilicate type 3.3 were  
137 filled with 50 mL of similar buffered solution as above and spiked either with atrazine (90  $\mu$ M) or  
138 *S*-metolachlor (70  $\mu$ M). Beakers were placed into the light-proof box, irradiated on the top, and  
139 sequentially removed to determine pesticide degradation rates. Light intensity within the box was  
140 homogeneous ( $83 < I_{\text{average}} < 121\%$ ; Fig. S2 in the ESI†). Control experiments without pesticides  
141 showed no cross-contamination. In this case, the photon fluence rate was not determined  
142 because the experiments were designed to evaluate the effect of the irradiation wavelength on  
143 atrazine and *S*-metolachlor isotope fractionation induced by photodegradation and not to derive  
144 degradation rates.

145

## 146 Analytical section

147 **Pesticide extraction.** Solid phase extraction (SPE) of pesticides was carried out using SolEx C18  
148 cartridges (1 g, Dionex, CA, USA) and an AutroTrace 280 SPE system (Dionex, CA, USA) as described  
149 elsewhere.<sup>27</sup> This procedure led to quantitative extraction ( $\eta \approx 100\%$ ) and did not result in  
150 significant C and N isotope fractionation for atrazine and *S*-metolachlor ( $|\Delta\delta^{13}\text{C}| =$   
151  $|\delta^{13}\text{C}_{EA-IRMS} - \delta^{13}\text{C}_{GC-IRMS}| = 0.6 \pm 0.2\text{‰}$  and  $|\Delta\delta^{15}\text{N}| = 0.3 \pm 0.2\text{‰}$ ).<sup>27</sup>

152

153 **Chemical analysis and pesticide quantification.** The ionic composition of irradiated solutions was  
154 determined by ion-chromatography (ICS-51000, Dionex) for main anions and cations and by Total  
155 Organic Carbon analyzer (TOC-V CPH, Shimadzu) for the C content in DOM. *pH* was measured  
156 using a 350i WTW *pH*-meter and a SenTix electrode. Absorption spectra of pesticides, NIT and  
157 DOM solutions were measured using a UV-VIS Shimadzu UV 1700 spectrophotometer over the

158 range 200 to 500 nm with a 1 nm resolution or taken from the literature whenever available (Fig.  
159 S3 in the ESI†).

160 Atrazine and *S*-metolachlor were quantified in selected-ion-monitoring (SIM) mode by gas-  
161 chromatography (GC, Trace 1300, Thermo Fisher Scientific) coupled with a mass-spectrometer  
162 (MS, ISQ™, Thermo Fisher Scientific), as previously described<sup>27</sup> and detailed in the ESI†. Atrazine  
163 and *S*-metolachlor TPs were identified by target screening using a liquid-chromatography coupled  
164 with a quadrupole time of flight high-resolution mass spectrometer (LC/Q-TOF) following the  
165 methodology described elsewhere.<sup>28</sup> A suspected list of molecules used for screening of TPs was  
166 generated using pathway prediction systems (UM-PPS, Metabolite Predict 2.0, META Ultra 1.2,  
167 Meta PC 1.8.1) and by reviewing the literature.<sup>29</sup> Tentative candidate molecules were assigned  
168 using the criteria of mass deviation ( $\Delta m/z$ ) below 3 ppm and mSigma value below 30. Whenever  
169 available, suspected molecule identifications were confirmed by matching residence times (RT  
170 <0.2 min) using analytical standards.

171

172 **Analysis of C and N stable isotope composition of pesticides.** C and N stable isotope ratios ( $\delta^{13}C$   
173 and  $\delta^{15}N$ ) of atrazine and *S*-metolachlor were measured using a GC-C-IRMS system consisting of  
174 a gas chromatograph (TRACE™ Ultra, ThermoFisher Scientific, Germany) coupled via a GC  
175 IsoLink/Conflow IV interface with an isotope ratio mass spectrometer (DeltaV Plus, ThermoFisher  
176 Scientific, Germany), and configured as described elsewhere<sup>27</sup> and detailed in the ESI†.

177  $\delta^{13}C$  and  $\delta^{15}N$  values were normalized by the Vienna Pee Dee Belemnite (VPDB) standard for C  
178 and by air for N as follows:

$$\delta^hX = 1000 \times (R_{sample}/R_{standard} - 1) \quad (1)$$

179 where  $\delta^hX$  is expressed in per thousand (‰) and  $R$  refers to the ratio of heavy ( $h$ ) to light ( $l$ )  
180 isotopes of the element  $X$  ( $^hX/{}^lX$ ) in the analyzed samples and the international standards.  
181 Samples were injected in triplicate and  $\delta^{13}C$  and  $\delta^{15}N$  values are reported as the arithmetic  
182 mean. Each measurement was within the linearity ranges for C and N. A set of in-house benzene,  
183 toluene, ethylbenzene and xylene (BTEX) (for C), caffeine (IAEA 600, for N) and pesticide (for C and  
184 N) standards with known isotopic composition was measured at least every ten injections to  
185 control the measurement quality. Reference  $\delta^{13}C$  and  $\delta^{15}N$  values of BTEX, caffeine and pesticide  
186 standards were determined using an elemental analyzer-isotope ratio mass spectrometer (Flash  
187 EA IsoLink™ CN IRMS, Thermo Fisher Scientific, Bremen, Germany). An analytical uncertainty of  
188  $1\sigma_{\delta^{13}C} \leq 0.5\text{‰}$  ( $n = 43$ ) and  $1\sigma_{\delta^{15}N} < 0.6\text{‰}$  ( $n = 72$ ) was attributed to each measurement,  
189 corresponding to the long-term accuracy and reproducibility of pesticide standards measured  
190 across the analytical sessions.

191

## 192 **Data Analysis**

193 Pesticide degradation followed the linearized pseudo-first order equation ( $R^2 > 0.82$ ,  $p < 0.05$ ,  $n > 5$ ).  
194 Degradation rates ( $k_{deg}$ ) were normalized by the mean irradiation intensity (Table S2 in the ESI†)  
195 according to eq. 2, allowing comparison among experiments. Degradation rates presented below  
196 refer to the normalized value,  $k_{eff}$ :

$$k_{eff} = \frac{I_{exp}}{I_{max}} \times k_{deg} \quad (2)$$

197 where  $I_{exp}$  and  $I_{max}$  stand for the light intensities measured during each experiment and the  
198 maximal inter-experiment value used as the reference for normalization.

199 The Rayleigh equation (eq. 3) was used to relate pesticide degradation to changes in stable isotope  
200 ratios of the non-degraded fraction of atrazine and S-metolachlor. Bulk isotope enrichment factor  
201 ( $\varepsilon_{bulk}$ ) for C and N ( $\varepsilon_C$  and  $\varepsilon_N$ ) were derived from the linearized Rayleigh equation and were not  
202 forced through the origin.<sup>30</sup> Isotope enrichment factors were only reported when the regression  
203 with the linearized Rayleigh equation was significant ( $p < 0.05$ ).

204

$$\frac{\delta^h X_t + 1000}{\delta^h X_0 + 1000} = \frac{C_t}{C_0}^{\frac{\varepsilon_{bulk}}{1000}} \quad (3)$$

205  $\delta^h X_0$  and  $\delta^h X_t$  are expressed in ‰ and refer, respectively, to the initial and current isotope  
206 composition of atrazine or S-metolachlor (eq. 1).  $C_t/C_0$  refers to the non-degraded fraction of  
207 atrazine or S-metolachlor. Correction of  $\varepsilon_{bulk}$  accounting for repetitive sampling in batch  
208 experiments were deemed irrelevant here as they systematically fell within the regression  
209 confidence interval.<sup>31</sup>

210 In addition to  $\varepsilon_{bulk}$ , dual-isotope plots with  $\delta^{15}N$  versus  $\delta^{13}C$  ( $\Lambda_{N/C}$ , eq. 4), reflecting changes of  
211 the isotope ratios of each element, were established to compare transformation pathways in  
212 laboratory experiments and the environment.<sup>13, 32</sup>  $\Lambda_{N/C}$  values were estimated using the York  
213 regression (R package geostats v1.3) accounting for uncertainty measurements of both C and N.<sup>33</sup>

$$\Lambda_{N/C} = \frac{\Delta\delta^{15}N}{\Delta\delta^{13}C} \approx \frac{\varepsilon_N}{\varepsilon_C} \quad (4)$$

214 All statistical analysis and regressions were performed in R version 3.6.3.<sup>34</sup> Data from linear  
215 regression (i.e.,  $k_{eff}$ ,  $\varepsilon_C$  and  $\varepsilon_N$ ) are reported with a 95% confidence interval.

216

## 217 Results and discussion

### 218 Effects of hydrochemistry on photodegradation rates under simulated sunlight

219 Nitrates and DOM under simulated sunlight affected atrazine and S-metolachlor  
220 photodegradation rates. Direct photodegradation in UW (DIR) exhibited the fastest degradation  
221 rates for both pesticides with  $k_{ATZ,DIR} = (6.6 \pm 0.4) \times 10^{-6} \text{ s}^{-1}$  (half-life;  $DT_{50} = 29.0 \pm 1.7 \text{ h}$ ) and  
222  $k_{SMET,DIR} = (3.3 \pm 0.2) \times 10^{-6} \text{ s}^{-1}$  ( $DT_{50} = 58.8 \pm 3.2 \text{ h}$ ). Atrazine was slightly more sensitive to direct  
223 photodegradation than S-metolachlor. Degradation half-lives ranged between 7 to 40 h for  
224 atrazine and between 30 to 87 h for S-metolachlor, and were within the same order of magnitude  
225 as previously reported half-lives.<sup>5, 7, 12, 35</sup> Differences in pesticide half-lives among the experiments  
226 may be due to different light spectra and power in the experiments where atrazine and S-  
227 metolachlor absorbed light in the near UV, overlapping with the lamp radiation spectrum (<320  
228 nm; Fig. S3 and Fig. S4 in the ESI<sup>+</sup>).

229 In contrast, the photodegradation rates of atrazine and S-metolachlor were, respectively, 4.1 and  
230 3.0 times lower in the experiments with DOM (5.4 mg C L<sup>-1</sup>), with or without nitrates (20 mg L<sup>-1</sup>),  
231 than in the UW experiments. This supports the notion that SRFA reduce atrazine and S-  
232 metolachlor photodegradation in surface waters at typical DOM contents.<sup>9, 10</sup> However,  
233 photodegradation rates were similar in experiments with nitrates only and with direct  
234 photodegradation ( $k_{ATZ,NIT}/k_{ATZ,DIR} = 0.8$  and  $k_{SMET,NIT}/k_{SMET,DIR} = 1.0$ ). The reaction rates  
235 increased in the experiment with both nitrates and SRFA ( $k_{ATZ,TOT}/k_{ATZ,SRFA} = 2.1$  and  
236  $k_{SMET,TOT}/k_{SMET,SRFA} = 1.2$ ). This indicates an oxidation of atrazine and S-metolachlor with HO•  
237 originating from nitrate irradiation. DOM and nitrates in surface waters have a similar  
238 photosensitizing or inhibitory effect on atrazine and S-metolachlor photodegradation. Indeed,  
239 atrazine and S-metolachlor have similar absorption spectra in the near UV range and very similar

240 one-electron oxidation potentials ( $E1_{S\text{-metolachlor}} = -2.40$  V vs NHE and  $E1_{\text{atrazine}\cdot} = -2.41$  V vs  
 241 NHE). It is worth noting that the one-electron oxidation potential is often used as an indicator of  
 242 the reaction potential of organic contaminants with  $^3\text{DOM}^*$  and  $\text{HO}\cdot$ .<sup>9, 11, 36</sup>  
 243 Photochemical predictions (eq. 5) allowed to infer the contribution of direct and indirect  
 244 photodegradation. The equation 5 teases apart the contribution of direct and indirect  
 245 photodegradation from the measured degradation rates (i.e.,  $\text{HO}\cdot$  and  $^3\text{DOM}^*$  mediated).<sup>5, 37, 38</sup>  
 246 Carbonate radicals ( $\text{CO}_3\cdot^-$ ) were not included as potentially relevant photosensitizers because  
 247 oxidation of atrazine and anilines with  $\text{CO}_3\cdot^-$  under simulated sunlight remains limited, even in  
 248 carbonate-rich surface waters ( $[\text{HCO}_3^-]$  and  $[\text{CO}_3^{2-}] \approx 10$  times higher than in our conditions).<sup>39</sup>  
 249 However, carbonates were considered as potential quenchers of  $\text{HO}\cdot$ .<sup>5</sup> The calculation procedure  
 250 and parameters are summarized in the ESI<sup>†</sup> Table S4.

$$\begin{aligned} \frac{dC}{dt} &= -k_{obs} \times C \\ &= -\left(k_{dir} + k_{\text{HO}\cdot} \times [\text{HO}\cdot]_{ss} + k_{^3\text{DOM}^*} \times [^3\text{DOM}^*]_{ss} + k_{^1\text{O}_2} \times [^1\text{O}_2]_{ss}\right) \quad (5) \\ &\quad \times C \end{aligned}$$

251  $C$  stands for pesticide concentration, and  $k_{obs}$  for the measured degradation rate ( $\text{s}^{-1}$ ), which can  
 252 be expressed as the sum of both direct ( $k_{dir}$ ) and various indirect pathways ( $k_{\text{HO}\cdot}$ ,  $k_{^3\text{DOM}^*}$  and  
 253  $k_{^1\text{O}_2}$ ). The latter degradation rates are second-order, and depend on the steady-state  
 254 concentrations of the short-lived reactive intermediates ( $[\text{HO}\cdot]_{ss}$ ,  $[^1\text{O}_2]_{ss}$  and  $[^3\text{DOM}^*]_{ss}$ ).  
 255 The observed and predicted degradation rates were similar. This suggests that the dominant  
 256 photodegradation pathway could be identified in all experiments (Fig. 1; Table S5 in the ESI<sup>†</sup>).  
 257 Nitrate-mediated photodegradation contributed to 60% of atrazine and 90% of *S*-metolachlor  
 258 photodegradation in TOT conditions. Nitrate-mediated photodegradation is thus expected to

259 dominate in agriculturally impacted surface waters. Although competing for UV light and limiting  
260 direct photodegradation, SRFA favored indirect photodegradation with  $^3\text{DOM}^*$  and  $\text{HO}\bullet$ .  
261 Accordingly, atrazine was slightly more sensitive than *S*-metolachlor to oxidation by  $^3\text{DOM}^*$ . In  
262 contrast,  $\text{HO}\bullet$  affected mostly *S*-metolachlor. Nitrate-mediated photodegradation was hampered  
263 in the TOT experiment in comparison with the NIT experiment. Indeed, DOM at  $5.4 \text{ mg}_C \text{ L}^{-1}$  not  
264 only competes for light irradiance with nitrates but also quenches  $\text{HO}\bullet$ . This is expected to reduce  
265 nitrate photosensitizing, as observed in the NIT experiment.<sup>10, 40</sup> In addition, direct  
266 photodegradation rates of both atrazine and *S*-metolachlor were 10 to 30 times slower in the SRFA  
267 than in the DIR experiments. Indeed, UV light absorption by DOM limited direct herbicide  
268 photodegradation. Finally,  $^1\text{O}_2$  stemming from reactions between dissolved oxygen and  $^3\text{DOM}^*$   
269 did not significantly contribute to herbicide degradation rates (<2% for atrazine and <4% for *S*-  
270 metolachlor). In aqueous solutions,  $^1\text{O}_2$  reaction with pesticides remains limited since water  
271 immediately scavenges most of the produced  $^1\text{O}_2$ .<sup>38</sup>

272

273

274

275

276

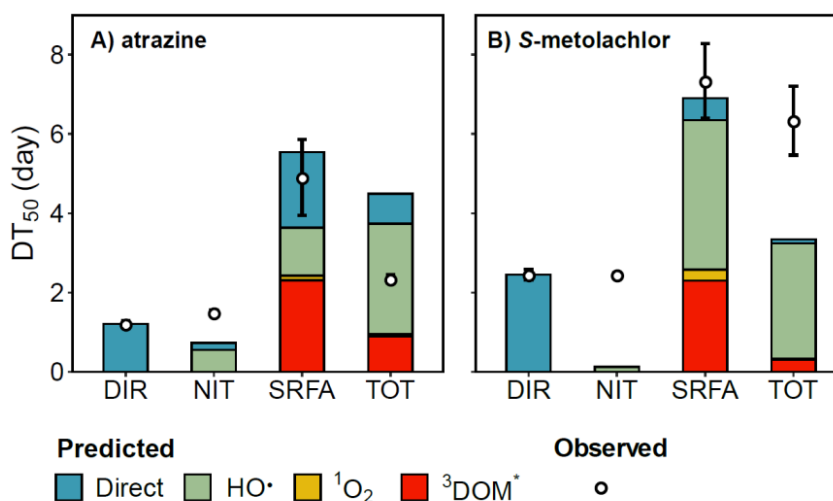
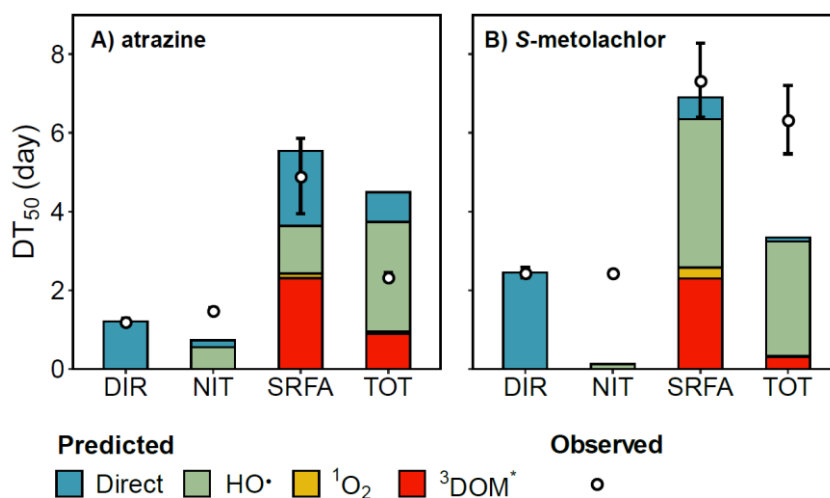
277

278

279

280

281



285 **Fig. 1.** Observed and predicted half-lives ( $DT_{50}$ ) of A) atrazine and B) S-metolachlor under  
 286 simulated sunlight. Predicted contributions of direct and indirect pathways ( $HO\cdot$ ,  $^1O_2$  and  $^3DOM^*$ )  
 287 to the total pesticide photodegradation is displayed within the stacked bars. Photolysis condition:  
 288 DIR: direct photodegradation, NIT: effect of nitrates, SRFA: effect of DOM and TOT: combined  
 289 effects of nitrates and DOM.  $DT_{50}$  values were calculated from degradation rates according to  
 290  $DT_{50} = \ln(2)/k$ . Error bars correspond to the 95% confidence interval.

292

293 Altogether, both direct and nitrate-mediated photodegradation can transform atrazine and S-  
294 metolachlor in agriculturally impacted surface waters. However, DOM competes for UV light  
295 absorption with pesticides and nitrates, which greatly reduces the transformation potential of  
296 pesticides. Pesticides with a light absorption spectrum in the near UV, such as atrazine, are thus  
297 less impacted. On the other hand, nitrates ( $20 \text{ mg L}^{-1}$ ) promote the generation of  $\text{HO}\bullet$ , which  
298 partly compensate for the UV light competition caused by DOM absorption.

299

### 300 **Formation of transformation products during photodegradation**

301 Transformation products (TPs) were analyzed in samples displaying a similar extent of  
302 photodegradation ( $\approx 80\%$ ). Atrazine irradiation led to desethylatrazine (DEA) and  
303 desisopropylatrazine (DIA) in all experiments. In contrast, 2-hydroxyatrazine (A-OH) was only  
304 detected in the direct photodegradation experiment (Fig. 2A).<sup>41</sup> A-OH is also reported during biotic  
305 hydrolysis.<sup>42</sup> Indirect photolysis may proceed through atrazine oxidation at the *N*-ethyl and *N*-  
306 isopropyl group by  $^3\text{DOM}^*$  and  $\text{HO}\bullet$ .<sup>41</sup> Non-selective attacks of  $\text{HO}\bullet$  on the *N*-ethyl and *N*-isopropyl  
307 groups may thermodynamically favor the formation of DEA since weaker N–C bond dissociation  
308 energy is associated with the *N*-ethyl group.<sup>43</sup> A steric effect is also expectedly favoring the  
309 formation of DEA as the isopropyl group is less reactive than the ethyl group.<sup>44</sup> On the other hand,  
310 the intermediates formed during the hydrogen abstraction by  $\text{HO}\bullet$  can electronically favor DIA  
311 formation due to the weaker C–H bond, and weaker intermediate stabilization by the isopropyl  
312 group than by the ethyl group.<sup>45</sup>

313

314 Four TPs of *S*-metolachlor were identified (Fig. 2B). Hydroxymetolachlor was observed in neither  
315 the DIR254 nor DIR experiments, although it was reported in previous studies<sup>12, 47, 48</sup> as a major TP  
316 formed during direct photodegradation of metolachlor. We postulate that hydroxymetolachlor  
317 was further degraded into secondary TPs after 80% degradation of *S*-metolachlor. In the SRFA and  
318 DIR experiments, only metolachlor oxalinic acid (OXA) was observed, whereas in NIT and TOT  
319 experiments, no TPs could be detected. This suggests that *S*-metolachlor was easily oxidized by  
320 <sup>3</sup>DOM\* and HO• into *S*-metolachlor OXA, its acidic form. In the presence of nitrates, the large and  
321 constant generation of nonselective HO• may favor fast degradation of *S*-metolachlor OXA.<sup>12</sup> This  
322 can explain the absence of TPs in the NIT and TOT experiments. The absence of TPs in the NIT and  
323 TOT experiments also supports the idea that nitrates mainly contribute to *S*-metolachlor  
324 photodegradation, even with 5.4 mg<sub>C</sub> L<sup>-1</sup> of DOM.

325 It is worth noting that the diversity of detected TPs was the highest for both atrazine and *S*-  
326 metolachlor during irradiations at  $\lambda = 254$  nm in the DIR254 experiments (Fig. 2B). In the case of  
327 *S*-metolachlor, metolachlor CGA 37735, metolachlor CGA 50267 and MET-G<sup>46</sup> were specific  
328 suspected TPs in the DIR254 experiments. However, only metolachlor CGA 37735 could be  
329 confirmed with analytical standards. This suggests that the spectrum of degradation pathways  
330 associated with monochromatic UV light is wider than that with simulated sunlight. In addition,  
331 specific TPs may be produced from the degradation of the first generation of TPs.

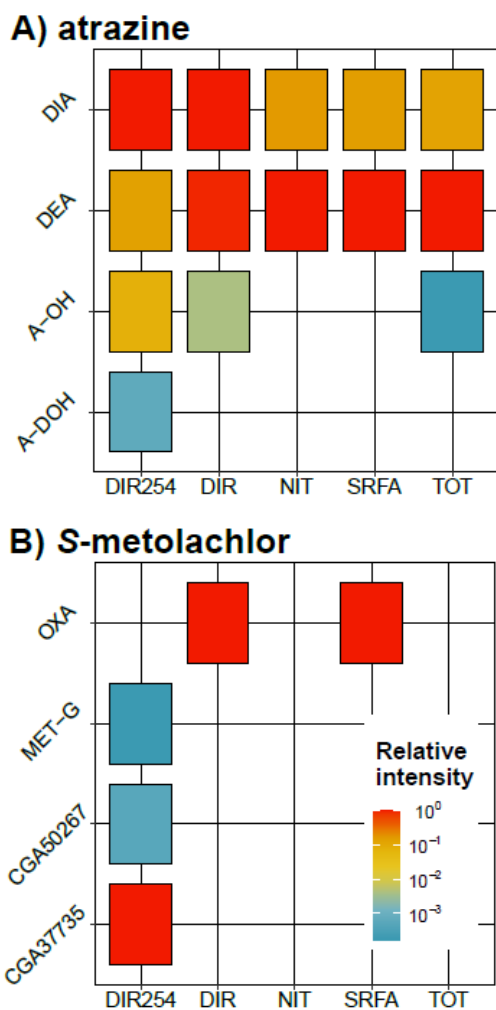
332

333

334

335

336



337

338 Fig. 2 Transformation products for A) atrazine and B) S-metolachlor in photolysis experiment.

339 Relative intensity refers to the peak amplitude of transformation product normalized by the

340 intensity of the dominant transformation product peak for each sample. Photolysis condition are:

341 DIR254: direct photodegradation at 254 nm, DIR: direct photodegradation under simulated

342 sunlight, NIT: effect of nitrates, SRFA: the effect of DOM, and TOT: concomitant effects of nitrates

343 and DOM together. TPs are: DIA: desisopropyl atrazine, DEA: desethyl atrazine, A-OH: hydroxyl

344 atrazine and A-DOH: desethyl 2 hydroxy atrazine, OXA: metolachlor oxalinic acid, MET-G: 1-(1-

345 methoxypropan-2-yl)-5,9-dimethyl-1,5-dihydro-4,1-benzoxazepin-2(3H)-one found by Lui et al.,<sup>45</sup>

346 CGA37735: metolachlor CGA 37735 and CGA50267: metolachlor CGA 50267.

347

348 Altogether, direct and indirect photodegradation pathways produce slightly different patterns of  
349 TPs. While the dechlorinated compound A-OH features direct photodegradation for atrazine,  
350 oxidized compounds (e.g., atrazine DEA and DIA and S-metolachlor OXA) are more likely to  
351 predominate in agriculturally impacted surface waters. However, TPs are likely transient and  
352 rapidly degraded into secondary and unidentified TPs, as shown during S-metolachlor  
353 photodegradation. TP patterns were identical for atrazine in the NIT and SRFA experiments,  
354 although <sup>3</sup>DOM\* oxidation is expected to prevail over HO•. Similarly, indirect photodegradation  
355 of S-metolachlor did not generate specific patterns of TPs. Interestingly, S-metolachlor ESA was  
356 not detected during either direct or indirect photodegradation. Since metolachlor ESA is  
357 frequently measured in the environment and is neither a transformation product associated with  
358 hydrolysis<sup>27</sup> or photodegradation, its recurrent detection may indicate S-metolachlor  
359 biodegradation.

360

361

## 362 **C and N isotope fractionation to trace atrazine and S-metolachlor photodegradation**

363 *Direct photodegradation experiments.* Direct photolysis of atrazine in the DIR254 experiment with  
364 a low-pressure mercury lamp caused an inverse isotope fractionation for both C and N ( $\Delta_{N/C}$  =  
365  $1.17 \pm 0.11$ ; Table 1). This is consistent with previous observations from Hartenbach et al.<sup>17</sup> ( $\Delta_{N/C}$   
366 =  $1.05 \pm 0.14$ ). However, isotope enrichment factors ( $\epsilon_C = 2.7 \pm 0.3\text{‰}$  and  $\epsilon_N = 2.4 \pm 0.3\text{‰}$ ) were  
367 less pronounced in the present study than in Hartenbach et al.<sup>17</sup> The lamp emission spectra and  
368 light path lengths may affect stable isotope fractionation. Indeed, the cut-off of light emission is  
369 >254 nm and the light path length in Hartenbach et al.<sup>17</sup> was smaller (1.4 cm) than in our study

370 (light path length = 4.9 cm). Hence, the contribution of the secondary band wavelength (>300 nm;  
371 Table S3, ESI<sup>+</sup>) may be higher in the DIR254 experiment. Assuming that wavelengths above 254  
372 nm do not cause significant isotope fractionation, different cut-offs and light path lengths in the  
373 two setups can lead to slightly different extents of isotope fractionation ( $\Delta\epsilon_C$  of 1.3).

374 The inverse C isotope fractionation of atrazine cannot be explained by the cleavage of the C–N  
375 bond at the *N*-ethyl or *N*-isopropyl group. Indeed, cleavage at the *N*-ethyl or *N*-isopropyl group  
376 leading to DEA and DIA should reflect a normal primary isotope effect.<sup>13</sup> Two non-exclusive  
377 hypotheses may explain the isotope fractionation patterns in the DIR254 experiments. First,  
378 successive steps of intersystem crossing before atrazine dechlorination can lead to an inverse  
379 isotope fractionation during direct photolysis of atrazine.<sup>17</sup> The inverse C isotope fractionation for  
380 atrazine in the DIR254 experiment is due to the generation of a singlet state radical stabilized by  
381 the ring delocalization. The excited singlet state then undergoes an intersystem crossing toward  
382 a triplet state and hydrolyzes to form A-OH. The likelihood of recombination back to their original  
383 state is higher for the light C isotope in the C–Cl bond, leading to an inverse C isotope  
384 fractionation.<sup>17, 19</sup> The same mechanism has been suggested to result in an inverse N isotope  
385 fractionation for atrazine. Second, a magnetic mass-independent isotope effect (MIE) involving  
386 spin carrying nuclei and unpaired electrons may also cause an inverse isotope fractionation.<sup>22, 49</sup>

387 In contrast, *S*-metolachlor featured a less pronounced and inverse C and stronger N isotope  
388 fractionation ( $\Delta_{N/C} = -4.24 \pm 0.22$ ) than atrazine. A similar nucleophilic substitution of the chlorine  
389 atom by a hydroxyl group at the C–Cl bond is expected for the formation of the MET-OH. However,  
390 it is *a priori* unlikely because the reactive site of *S*-metolachlor is too far from the ring.

391

392

393 **Table 1.** C and N isotope difference ( $\Delta\delta^{13}C$  and  $\Delta\delta^{15}N$ ), isotope enrichment factors ( $\epsilon$ ) and lambda values  
 394 ( $\Lambda_{N/C}$ ) for atrazine and *S*-metolachlor

pesticide	experiment ( $C_{t=end}/C_0$ )	$\Delta\delta^{13}C$ (‰)	$\Delta\delta^{15}N$ (‰)	$\epsilon_C$ (‰)	$\epsilon_N$ (‰)	$\Lambda_{N/C}$
atrazine	DIR 254 (0.01)	-8.1	-10.8	$+2.7 \pm 0.3^*$	$+2.4 \pm 0.3^*$	$+1.17 \pm 0.11$
	DIR (0.10)	-0.3	-0.5	n.s.	n.s.	n.c.
	NIT (0.01)	0.4	-2.0	n.s.	$+0.7 \pm 0.3$	n.c.
	SRFA (0.03)	-0.7	-0.8	n.c.	$+0.6 \pm 0.2$	n.c.
	TOT (0.02)	-0.6	-4.1	$+0.1 \pm 0.1$	$+0.9 \pm 0.6$	$+6.0 \pm 2.2$
<i>S</i> -metolachlor	DIR 254 (0.01)	-2.3	4.5	$+0.8 \pm 0.1^*$	$-2.6 \pm 0.7^*$	$-4.24 \pm 0.22$
	DIR (0.2)	0.2	1.0	n.s.	n.s.	n.c.
	NIT (0.02)	0.5	3.3	n.s.	$-0.8 \pm 0.1$	n.c.
	SRFA (0.06)	-0.6	1.8	n.c.	$-0.7 \pm 0.4$	n.c.
	TOT (0.06)	0.2	1.8	n.c.	$-0.7 \pm 0.1$	n.c.

395  $\Delta\delta = \delta(t) - \delta(t=0)$ . isotope enrichment factors ( $\epsilon$ ) are reported with their uncertainties corresponding to  
 396 the 95% confidence interval from the regression analysis. n.s.: not significant ( $p>0.05$ ). n.c.: not computed.  
 397 Rayleigh plots are presented in the ESI† Fig. S5 & S6. \*  $\epsilon$  calculated for data with  $C_t/C_0>0.2$  only as  
 398 recommended by<sup>50,51</sup>

399

400 Direct photodegradation under simulated sunlight (DIR) led to non-significant C and N isotope  
 401 fractionation for both atrazine et *S*-metolachlor (Table 1). This suggests that C isotope  
 402 fractionation associated with direct photodegradation under simulated sunlight of organic  
 403 micropollutants remains limited. This is in line with preliminary evidence from diclofenac  
 404 photolysis.<sup>16</sup> Most importantly, our results indicate that photo-induced C and N isotope

405 fractionation depends on the irradiation wavelength. Similar results have been reported by  
406 Willach et al.<sup>18</sup> for the antibiotic sulfamethoxazole under broad and cut-off light spectrums. The  
407 Xe lamp emits light over a broad and continuous range of wavelengths and energies from the near  
408 UV ( $\lambda > 270$  nm) to the near-infrared ( $\lambda < 600$  nm), whereas the Hg lamp generates a single-band  
409 UV light ( $\lambda = 254$  nm). Consequently, the Xe lamp emission may generate a miscellaneous  
410 population of excited triplet states. This presumably affected the photolytic dechlorination of 4-  
411 Cl-aniline and led to varying and compensating C and N stable isotope fractionation caused by a  
412 spin selective isotope effect.<sup>50</sup> Hence, the average isotope composition of the residual fraction of  
413 atrazine and S-metolachlor may reflect multiple and co-occurring photodegradation reactions  
414 under simulated sunlight. Interestingly, atrazine direct photolysis quantum yield also depended  
415 on the wavelength, with values ranging from 0.0158 to 0.0196 for simulated sunlight and from  
416 0.035 to 0.060 for 254 nm irradiation.<sup>7</sup> This emphasizes that the photodegradation pathways are  
417 wavelength-dependent, while each pathway is characterized by a specific isotope fractionation  
418 and associated quantum yield.

419

420 *Indirect photodegradation experiments.* In the indirect photodegradation experiments (NIT, SRFA  
421 and TOT), only slight C and N isotope fractionation were observed, even at the latest stage of the  
422 reactions (>80% of degradation; Fig. S5 & S6 in the ESI<sup>†</sup>). Thus, the uncertainties associated with  
423 the isotope enrichment factors ( $\epsilon$ ) were larger for the indirect than for the direct  
424 photodegradation experiments, and corresponding  $\epsilon$  should be interpreted with caution.

425 C isotope fractionation was insignificant in both the NIT and TOT experiments under simulated  
426 sunlight, except for atrazine under in the TOT experiment. Similar N isotope fractionation patterns  
427 were observed in both the NIT and TOT experiments ( $\epsilon_N^{TOT} / \epsilon_N^{NIT} = 1.3 \pm 0.5$  for atrazine

428 and  $\varepsilon_N^{TOT} / \varepsilon_N^{NIT} = 0.9 \pm 0.2$  for *S*-metolachlor). However, the N isotope fractionation was inverse for  
429 atrazine and normal for *S*-metolachlor. Similar N isotope fractionation for atrazine and *S*-  
430 metolachlor supports the idea that nitrate-mediated photodegradation predominates in  
431 agriculturally impacted surface waters, even in the presence of  $5.4 \text{ mg}_C \text{ L}^{-1}$  of DOM. Accordingly,  
432  $\varepsilon_N$  for atrazine and *S*-metolachlor in the NIT experiments represent reference factors for HO•  
433 oxidation in the presence of nitrates.

434 In the SRFA experiments, where  $^3\text{DOM}^*$  oxidation and HO• presumably drove the indirect  
435 photodegradation, only N isotope fractionation was observed for atrazine ( $\varepsilon_N = 0.6 \pm 0.2\text{‰}$ ) and  
436 *S*-metolachlor ( $\varepsilon_N = -0.7 \pm 0.4\text{‰}$ ). Low N isotope fractionation upon  $^3\text{DOM}^*$  oxidation is consistent  
437 with the absence of C–N bond cleavage during *S*-metolachlor dechlorination leading to OXA. In  
438 addition, similar N fractionation in the NIT and SRFA experiments ( $\varepsilon_N^{SRFA} / \varepsilon_N^{NIT} = 0.9 \pm 0.5$ ) for both  
439 atrazine and *S*-metolachlor suggest a significant contribution to the overall photodegradation of  
440 HO• radicals, generated by DOM irradiation (HO• = 54% and  $^3\text{DOM}^* = 33\%$ ). The inverse N isotope  
441 fractionation for atrazine also agrees with an oxidation by  $^3\text{DOM}^*$  at the *N*-ethyl or *N*-isopropyl  
442 side chain, leading to either DEA or DIA through single electron transfer.<sup>20, 53</sup> Accordingly, an  
443 inverse C isotope fractionation would be expected, which is not the case. The large collection of  
444 chromophores in natural DOM (i.e., SRFA) results in a wide panel of excited state reduction  
445 potentials for the oxidation of molecular bonds involving irrespectively heavy or light stable  
446 isotopes.<sup>10</sup> This hypothesis could be confirmed experimentally using Cs<sup>+</sup> as a quencher of excited  
447 singlet states to enhance the contribution of excited triplet states. The corresponding decrease of  
448  $\varepsilon_C$  and  $\varepsilon_N$  could then be followed up, as previously shown for 2-Cl-anilines.<sup>50</sup>

449

450

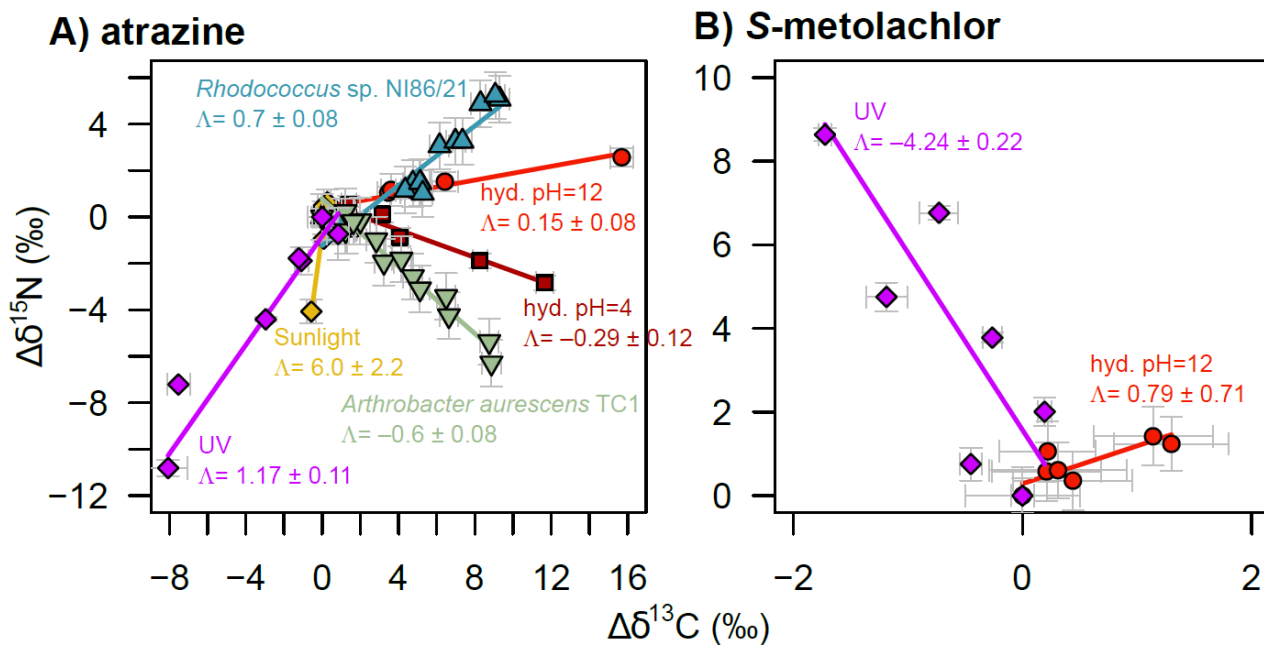
## 451 Implication for tracing photodegradation using CSIA in the environment

452 Photodegradation contributes to pesticide degradation to a similar or greater extent than  
453 biodegradation<sup>3</sup> in static surface waters (e.g., ponds, lakes, etc.) and rivers with long transit time.<sup>54</sup>

454 However, the contribution of photodegradation depends on the hydrochemistry and targeted  
455 pesticides. The direct photodegradation of atrazine and *S*-metolachlor was particularly fast,  
456 although it was slowed down by the UV light absorption caused by DOM. However, nitrate  
457 concentrations higher than 20 mg L<sup>-1</sup> can significantly enhance oxidation by producing HO•,  
458 counterbalancing the photodegradation inhibition caused by DOM in surface waters. Under  
459 simulated sunlight and environmentally-relevant hydrochemistry (*pH* = 8; 20 mg L<sup>-1</sup> of nitrates  
460 and 5.4 mg<sub>C</sub> L<sup>-1</sup> of DOM), half-lives of atrazine and *S*-metolachlor were as short as a few days  
461 ( $1 < DT_{50} < 10$  days). However, strong variations that occur naturally in solar irradiance in the UV  
462 region either due to gaseous light absorption by ozone at different altitudes or geographic  
463 locations, or to the rapid absorption of UV lights in the water, restrict our conclusions to shallow  
464 surface waters (i.e., <50 cm deep).<sup>55</sup> Altogether, this advocates to take more systematically into  
465 account the local irradiation spectrum and hydrochemical conditions to estimate the kinetics and  
466 the contribution of pesticide photodegradation.<sup>56</sup>

467 While CSIA offers a new opportunity to evaluate pesticide degradation in surface waters,  
468 identifying photodegradation pathways of micropollutants in the environment remains  
469 challenging.<sup>16,18</sup> Under simulated sunlight irradiation, the C and N isotope compositions of atrazine  
470 and *S*-metolachlor are not significantly affected by photodegradation, although photodegradation  
471 contributes significantly to pesticide degradation. Accordingly, changes in the C stable isotope  
472 ratios may mostly reflect atrazine or *S*-metolachlor biodegradation. Indeed, biodegradation is  
473 typically characterized by significant isotope fractionation (Fig. 3) in surface waters with high

474 nitrate and DOM concentrations. This is illustrated by the dual-element plots comparing N/C  
 475 isotope enrichment factors determined in this study with those from the literature (Fig. 3).  
 476



477

478 **Fig. 3** Dual C and N isotope plot for A) atrazine and B) S-metolachlor. Contrasted isotope  
 479 fractionation patterns are represented under biotic oxidative dealkylation by the bacterial strain  
 480 *Rhodococcus* sp. NI86/21, biotic hydrolysis with *Arthrobacter aureescens* TC1,<sup>56</sup> abiotic acid (pH=4)  
 481 and alkaline (pH=12) hydrolysis (hyd.)<sup>27</sup> and photodegradation for DIR254 and TOT condition (this  
 482 study).

483

484 However, relying solely on changes of N isotope ratios may not enable a univocal differentiation  
 485 of degradation pathways. For instance, atrazine photodegradation under DIR254 condition ( $\epsilon_N =$   
 486  $2.4 \pm 0.3\text{‰}$ ) and biodegradation ( $\epsilon_N = 2.3 \pm 0.3\text{‰}$ )<sup>56</sup> have identical  $\epsilon_N$ . This emphasizes the need  
 487 for multi-element isotope analysis (e.g., H, C, N and Cl) to elucidate degradation pathways.  
 488 Photodegradation pathways of atrazine and S-metolachlor mostly involve C–H and C–Cl bonds.<sup>16,</sup>

489 <sup>17</sup> In the future, multi-element isotope analysis of pesticides by CSIA from environmental samples  
490 may help to distinguish photodegradation pathways and evaluate the contribution of  
491 photodegradation to the overall dissipation.

## 492 **Conclusion**

493 This study highlights the relevance of direct and indirect photodegradation of pesticides in  
494 agriculturally impacted surface waters with nitrates and DOM. The irradiation source strongly  
495 influences the C and N isotope fractionation patterns while the hydrochemistry (i.e., nitrate, DOM)  
496 affects the degradation rates. Consequently, reference isotope enrichment factors to evaluate  
497 photodegradation in the environment with CSIA should be derived from laboratory experiments  
498 using simulated sunlight. In addition, the nature of DOM under different environmental contexts  
499 can affect the production of HO•, and thus alter stable isotope fractionation of pesticides.<sup>20, 50</sup>  
500 Although SRFA can serve as a model DOM representative of headwater rivers,<sup>9</sup> the effect of DOM  
501 characteristics on stable isotope fractionation during pesticide photodegradation should be  
502 further studied. Finally, recent developments on Cl-CSIA offer promising insights to investigate  
503 pesticide degradation pathways in surface waters using multi-element CSIA.<sup>57, 58</sup>

## 504 **Author Contributions**

505 Conceptualization: G.D., B.D., F.L, S.P., J.M. & G.I. Data curation, formal analysis and investigation:  
506 G.D. & B.D. Writing original draft: G.D & B.D. Writing review and editing: G.D., B.D., F.L, S.P., J.M.  
507 & G.I. Funding acquisition, project administration, supervision: G.I.

## 508 **Conflicts of interest**

509 There are no conflicts to declare.

## 510 **Acknowledgements**

511 G.D. was supported by the French Ministry for the Ecological Transition. B.D. was supported by a  
512 fellowship of the Région Grand Est and the AERM (France). This study was funded by the Region  
513 Grand Est, the Rhine-Meuse Water Agency (n°170293) as well as the National School for Water  
514 and Environmental Engineering (ENGEES). We acknowledge Jeroen E. Sonke (Laboratory for  
515 Environmental Geosciences, University of Toulouse) for lending the sunlight simulator, and  
516 Thomas Cottineau (Institute of Chemistry and Processes for Energy Environment and Health,  
517 University of Strasbourg), for his help in light spectrum characterization. We are grateful to Loic  
518 Maurer, Dimitri Heintz and Claire Villette (Laboratory of Plant Imaging and Mass Spectrometry,  
519 University of Strasbourg) for their help with TPs characterization. We gratefully acknowledge  
520 Jenna Lohmann and Elodie Passeport for enabling significant improvements of the manuscript.

## 521 **References**

- 522 1 R. M. de Souza, D. Seibert, H. B. Quesada, F. de Jesus Bassetti, M. R. Fagundes-Klen and R.  
523 Bergamasco, Occurrence, impacts and general aspects of pesticides in surface water: A review,  
524 *Process Saf. Environ. Prot.*, 2020, **135**, 22–37, DOI: 10.1016/j.psep.2019.12.035.
- 525 2 S. Stehle and R. Schulz, Agricultural insecticides threaten surface waters at the global scale, *Proc.*  
526 *Natl. Acad. Sci. U.S.A.*, 2015, **112**, 5750–5755, DOI: 10.1073/pnas.1500232112.
- 527 3 K. Fenner, S. Canonica, L. P. Wackett and M. Elsner, Evaluating pesticide degradation in the  
528 environment: Blind spots and emerging opportunities, *Science*, 2013, **341**, 752–758, DOI:  
529 10.1126/science.1236281.
- 530 4 C. K. Remucal, The role of indirect photochemical degradation in the environmental fate of  
531 pesticides: A review, *Environ. Sci. Process. Impacts*, 2014, **16**, 628–653, DOI: 10.1039/c3em00549f.

- 532 5 T. Zeng and W. A. Arnold, Pesticide photolysis in prairie potholes: Probing photosensitized  
533 processes, *Environ. Sci. Technol.*, 2013, **47**, 6735–6745, DOI: 10.1021/es3030808.
- 534 6 M. Celeiro, R. Facorro, T. Dagnac, V. J. P. Vilar and M. Llompart, Photodegradation of multiclass  
535 fungicides in the aquatic environment and determination by liquid chromatography-tandem mass  
536 spectrometry, *Environ. Sci. Pollut. Res.*, 2017, **24**, 19181–19193, DOI: 10.1007/s11356-017-9487-  
537 2.
- 538 7 B. Wu, W. A. Arnold and L. Ma, Photolysis of atrazine: Role of triplet dissolved organic matter and  
539 limitations of sensitizers and quenchers, *Water Res.*, 2021, **190**, 116659, DOI:  
540 10.1016/j.watres.2020.116659.
- 541 8 D. Vione, M. Minella, V. Maurino and C. Minero, Indirect photochemistry in sunlit surface waters:  
542 Photoinduced production of reactive transient species, *Chem. Eur. J.*, 2014, **20**, 10590–10606, DOI:  
543 10.1002/chem.201400413.
- 544 9 F. Leresche, U. von Gunten and S. Canonica, Probing the photosensitizing and inhibitory effects of  
545 dissolved organic matter by using *N,N*-dimethyl-4-cyanoaniline (DMABN), *Environ. Sci. Technol.*,  
546 2016, **50**, 10997–11007, DOI: 10.1021/acs.est.6b02868.
- 547 10 F. L. Rosario-Ortiz and S. Canonica, Probe compounds to assess the photochemical activity of  
548 dissolved organic matter, *Environ. Sci. Technol.*, 2016, **50**, 12532–12547, DOI:  
549 10.1021/acs.est.6b02776.
- 550 11 M. E. Karpuzcu, A. J. McCabe and W. A. Arnold, Phototransformation of pesticides in prairie  
551 potholes: Effect of dissolved organic matter in triplet-induced oxidation, *Environ. Sci. Process.*  
552 *Impacts*, 2016, **18**, 237–245, DOI: 10.1039/C5EM00374A.

- 553 12 A. D. Dimou, V. A. Sakkas and T. A. Albanis, Metolachlor photodegradation study in aqueous media  
554 under natural and simulated solar irradiation, *J. Agric. Food. Chem.*, 2005, **53**, 694–701, DOI:  
555 10.1021/jf048766w.
- 556 13 M. Elsner and G. Imfeld, Compound-specific isotope analysis (CSIA) of micropollutants in the  
557 environment — current developments and future challenges, *Curr. Opin. Biotechnol.*, 2016, **41**,  
558 60–72, DOI: 10.1016/j.copbio.2016.04.014.
- 559 14 M. Elsner, L. Zwank, D. Hunkeler and R. P. Schwarzenbach, A new concept linking observable stable  
560 isotope fractionation to transformation pathways of organic pollutants, *Environ. Sci. Technol.*,  
561 2005, **39**, 6896–6916, DOI: 10.1021/es0504587.
- 562 15 M. Thullner, F. Centler, H. H. Richnow and A. Fischer, Quantification of organic pollutant  
563 degradation in contaminated aquifers using compound specific stable isotope analysis - Review of  
564 recent developments, *Org. Geochem.*, 2012, **42**, 1440–1460, DOI:  
565 10.1016/j.orggeochem.2011.10.011.
- 566 16 M. P. Maier, C. Prasse, S. G. Pati, S. Nitsche, Z. Li, M. Radke, A. Meyer, T. B. Hofstetter, T. A. Ternes  
567 and M. Elsner, Exploring trends of C and N isotope fractionation to trace transformation reactions  
568 of diclofenac in natural and engineered systems, *Environ. Sci. Technol.*, 2016, **50**, 10933–10942,  
569 DOI: 10.1021/acs.est.6b02104.
- 570 17 A. E. Hartenbach, T. B. Hofstetter, P. R. Tentscher, S. Canonica, M. Berg and R. P. Schwarzenbach,  
571 Carbon, hydrogen, and nitrogen isotope fractionation during light-induced transformations of  
572 atrazine, *Environ. Sci. Technol.*, 2008, **42**, 7751–7756, DOI: 10.1021/es800356h.
- 573 18 S. Willach, H. V. Lutze, K. Eckey, K. Löppenberg, M. Lüling, J.-B. Wolbert, D. M. Kujawinski, M. A.  
574 Jochmann, U. Karst and T. C. Schmidt, Direct photolysis of sulfamethoxazole using various  
575 irradiation sources and wavelength ranges — insights from degradation product analysis and

- 576 compound-specific stable isotope analysis, *Environ. Sci. Technol.*, 2018, **52**, 1225–1233, DOI:  
577 10.1021/acs.est.7b04744.
- 578 19 N. Knossow, H. Siebner and A. Bernstein, Isotope analysis method for the herbicide bromoxynil  
579 and its application to study photo-degradation processes, *J. Hazard. Mater.*, 2020, **388**, 122036,  
580 DOI: 10.1016/j.jhazmat.2020.122036.
- 581 20 N. Zhang, J. Schindelka, H. Herrmann, C. George, M. Rosell, S. Herrero-Martín, P. Klán and H. H.  
582 Richnow, Investigation of humic substance photosensitized reactions via carbon and hydrogen  
583 isotope fractionation, *Environ. Sci. Technol.*, 2015, **49**, 233–242, DOI: 10.1021/es502791f.
- 584 21 E. J. Smith, W. Davison and J. Hamilton-Taylor, Methods for preparing synthetic freshwaters,  
585 *Water Res.*, 2002, **36**, 1286–1296, DOI: 10.1016/S0043-1354(01)00341-4.
- 586 22 M. Ratti, S. Canonica, K. McNeill, P. R. Erickson, J. Bolotin and T. B. Hofstetter, Isotope fractionation  
587 associated with the direct photolysis of 4-chloroaniline, *Environ. Sci. Technol.*, 2015, **49**, 4263–  
588 4273, DOI: 10.1021/es505784a.
- 589 23 European Environment Agency (EEA), The European environment – state and outlook 2020 :  
590 Knowledge for transition to a sustainable Europe, Copenhagen, DK, 2019.
- 591 24 P. A. Raymond and R. G. M. Spencer, in *Biogeochemistry of marine dissolved organic matter*  
592 (*Second edition*), eds. D. A. Hansell and C. A. Carlson, Academic Press, Boston, 2015, DOI:  
593 10.1016/B978-0-12-405940-5.00011-X, pp. 509–533.
- 594 25 D. Dulin and T. Mill, Development and evaluation of sunlight actinometers, *Environ. Sci. Technol.*,  
595 1982, **16**, 815–820, DOI: 10.1021/es00105a017.
- 596 26 J. R. Laszakovits, S. M. Berg, B. G. Anderson, J. E. O’Brien, K. H. Wammer and C. M. Sharpless, *p*-  
597 nitroanisole/pyridine and *p*-nitroacetophenone/pyridine actinometers revisited: Quantum yield

598 in comparison to ferrioxalate, *Environ. Sci. Technol. Let.*, 2017, **4**, 11–14, DOI:  
599 10.1021/acs.estlett.6b00422.

600 27J. Masbou, G. Drouin, S. Payraudeau and G. Imfeld, Carbon and nitrogen stable isotope  
601 fractionation during abiotic hydrolysis of pesticides, *Chemosphere*, 2018, **213**, 368–376, DOI:  
602 10.1016/j.chemosphere.2018.09.056.

603 28C. Villette, L. Maurer, A. Wanko and D. Heintz, Xenobiotics metabolization in *Salix alba* leaves  
604 uncovered by mass spectrometry imaging, *Metabolomics*, 2019, **15**, 122, DOI: 10.1007/s11306-  
605 019-1572-8.

606 29B. Droz, G. Drouin, L. Maurer, C. Villette, S. Payraudeau and G. Imfeld, Phase transfer and  
607 biodegradation of pesticides in water-sediment systems explored by compound-specific isotope  
608 analysis and conceptual modeling, *Environ. Sci. Technol.*, 2021, DOI: 10.1021/acs.est.0c06283.

609 30K. M. Scott, X. Lu, C. M. Cavanaugh and J. S. Liu, Optimal methods for estimating kinetic isotope  
610 effects from different forms of the Rayleigh distillation equation, *Geochim. Cosmochim. Acta*,  
611 2004, **68**, 433–442, DOI: 10.1016/S0016-7037(03)00459-9.

612 31D. Buchner, B. Jin, K. Ebert, M. Rolle, M. Elsner and S. B. Haderlein, Experimental determination of  
613 isotope enrichment factors - bias from mass removal by repetitive sampling, *Environ. Sci. Technol.*,  
614 2017, **51**, 1527–1536, DOI: 10.1021/acs.est.6b03689.

615 32R. S. Wijker, P. Adamczyk, J. Bolotin, P. Paneth and T. B. Hofstetter, Isotopic analysis of oxidative  
616 pollutant degradation pathways exhibiting large H isotope fractionation, *Environ. Sci. Technol.*,  
617 2013, **47**, 13459–13468, DOI: 10.1021/es403597v.

618 33A. S. Ojeda, E. Phillips, S. A. Mancini and B. S. Lollar, Sources of uncertainty in biotransformation  
619 mechanistic interpretations and remediation studies using CSIA, *Anal. Chem.*, 2019, **91**, 9147-  
620 9153, DOI: 10.1021/acs.analchem.9b01756.

- 621 34 R Core Team, R: A language and environment for statistical computing, <http://www.R-project.org>,  
622 (accessed 10 March 2018).
- 623 35 I. K. Konstantinou, T. M. Sakellarides, V. A. Sakkas and T. A. Albanis, Photocatalytic degradation of  
624 selected s-triazine herbicides and organophosphorus insecticides over aqueous TiO<sub>2</sub> suspensions,  
625 *Environ. Sci. Technol.*, 2001, **35**, 398-405, DOI: 10.1021/es001271c.
- 626 36 W. A. Arnold, One electron oxidation potential as a predictor of rate constants of N-containing  
627 compounds with carbonate radical and triplet excited state organic matter, *Environ. Sci. Process.*  
628 *Impacts*, 2014, **16**, 832–838, DOI: 10.1039/C3EM00479A.
- 629 37 M. Bodrato and D. Vione, APEX (Aqueous Photochemistry of Environmentally occurring  
630 Xenobiotics): a free software tool to predict the kinetics of photochemical processes in surface  
631 waters, *Environ. Sci. Process. Impacts*, 2014, **16**, 732–740, DOI: 10.1039/C3EM00541K.
- 632 38 E. M. L. Janssen, P. R. Erickson and K. McNeill, Dual roles of dissolved organic matter as sensitizer  
633 and quencher in the photooxidation of tryptophan, *Environ. Sci. Technol.*, 2014, **48**, 4916–4924,  
634 DOI: 10.1021/es500535a.
- 635 39 D. Vione, V. Maurino, C. Minero, M. E. Carlotti, S. Chiron and S. Barbati, Modelling the occurrence  
636 and reactivity of the carbonate radical in surface freshwater, *Comptes Rendus Chimie*, 2009, **12**,  
637 865–871, DOI: 10.1016/j.crci.2008.09.024.
- 638 40 J. R. Garbin, D. M. B. P. Milori, M. L. Simões, W. T. L. da Silva and L. M. Neto, Influence of humic  
639 substances on the photolysis of aqueous pesticide residues, *Chemosphere*, 2007, **66**, 1692–1698,  
640 DOI: 10.1016/j.chemosphere.2006.07.017.
- 641 41 A. Torrents, B. G. Anderson, S. Bilboulia, W. E. Johnson and C. J. Hapeman, Atrazine photolysis:  
642 Mechanistic investigations of direct and nitrate mediated hydroxy radical processes and the

643 influence of dissolved organic carbon from the Chesapeake Bay, *Environ. Sci. Technol.*, 1997, **31**,  
644 1476–1482, DOI: Doi 10.1021/Es9607289.

645 42 A. H. Meyer, H. Penning and M. Elsner, C and N isotope fractionation suggests similar mechanisms  
646 of microbial atrazine transformation despite involvement of different enzymes (AtzA and TrzN),  
647 *Environ. Sci. Technol.*, 2009, **43**, 8079–8085, DOI: 10.1021/es9013618.

648 43 K. P. C. Vollhardt and N. E. Schore, *Organic chemistry: Structure and function*, Freemann, W.H.,  
649 1999.

650 44 M. B. Smith and J. March, *March's advanced organic chemistry: Reactions, mechanisms, and*  
651 *structure*, John Wiley & Sons, Sixth Edition. edn., 2006.

652 45 C. J. Hapeman, J. S. Karns and D. R. Shelton, Total mineralization of aqueous atrazine in the  
653 presence of ammonium nitrate using ozone and *Klebsiella terrigena* (strain drs-i): mechanistic  
654 considerations for pilot scale disposal, *J. Agric. Food. Chem.*, 1995, **43**, 1383–1391, DOI:  
655 10.1021/jf00053a047.

656 46 S. Y. Liu, A. J. Freyer and J. M. Bollag, Microbial dechlorination of the herbicide metolachlor, *J.*  
657 *Agric. Food. Chem.*, 1991, **39**, 631–636, DOI: 10.1021/jf00003a038.

658 47 L. Gutowski, E. Baginska, O. Olsson, C. Leder and K. Kummerer, Assessing the environmental fate  
659 of S-metolachlor, its commercial product Mercantor Gold® and their photoproducts using a water-  
660 sediment test and in silico methods, *Chemosphere*, 2015, **138**, 847–855, DOI:  
661 10.1016/j.chemosphere.2015.08.013.

662 48 L. Gutowski, O. Olsson, C. Leder and K. Kümmerer, A comparative assessment of the  
663 transformation products of S-metolachlor and its commercial product Mercantor Gold® and their  
664 fate in the aquatic environment by employing a combination of experimental and in silico  
665 methods, *Sci. Total Environ.*, 2015, **506-507**, 369–379, DOI: 10.1016/j.scitotenv.2014.11.025.

- 666 49 A. L. Buchachenko, Mass-independent isotope effects, *J. Phys. Chem. B*, 2013, **117**, 2231–2238,  
667 DOI: 10.1021/jp308727w.
- 668 50 M. Ratti, S. Canonica, K. McNeill, J. Bolotin and T. B. Hofstetter, Isotope fractionation associated  
669 with the photochemical dechlorination of chloroanilines, *Environ. Sci. Technol.*, 2015, **49**, 9797–  
670 9806, DOI: 10.1021/acs.est.5b02602.
- 671 51 J. Bigeleisen and T. L. Allen, Fractionation of the Carbon Isotopes in Decarboxylation Reactions. IV.  
672 The Relative Rates of Decomposition of 1-C<sup>12</sup> and 1-C<sup>13</sup> Trichloroacetate Ions, *The Journal of*  
673 *Chemical Physics*, 1951, **19**, 760–764, DOI: 10.1063/1.1748348.
- 674 52 S. O. C. Mundle, B. S. Lollar and R. Kluger, in *Methods Enzymol.*, eds. M. E. Harris and V. E.  
675 Anderson, Academic Press, 2017, vol. 596, pp. 501–522.
- 676 53 A. H. Meyer, A. Dybala-Defratyka, P. J. Alaimo, I. Geronimo, A. D. Sanchez, C. J. Cramer and M.  
677 Elsner, Cytochrome P450-catalyzed dealkylation of atrazine by *Rhodococcus* sp. strain N186/21  
678 involves hydrogen atom transfer rather than single electron transfer, *Dalton Trans.*, 2014, **43**,  
679 12175–12186, DOI: 10.1039/c4dt00891j.
- 680 54 L. J. Fono, E. P. Kolodziej and D. L. Sedlak, Attenuation of wastewater-derived contaminants in an  
681 effluent-dominated river, *Environ. Sci. Technol.*, 2006, **40**, 7257–7262, DOI: 10.1021/es061308e.
- 682 55 R. P. Schwarzenbach, P. M. Gschwend and D. M. Imboden, *Environmental organic chemistry*, John  
683 Wiley & Sons, third edn., 2016.
- 684 56 J. N. Apell and K. McNeill, Updated and validated solar irradiance reference spectra for estimating  
685 environmental photodegradation rates, *Environ. Sci. Process. Impacts*, 2019, **21**, 427–437, DOI:  
686 10.1039/C8EM00478A.

- 687 57 C. Lihl, B. Heckel, A. Grzybkowska, A. Dybala-Defratyka, V. Ponsin, C. Torrentó, D. Hunkeler and M.  
688 Elsner, Compound-specific chlorine isotope fractionation in biodegradation of atrazine, *Environ.*  
689 *Sci. Process. Impacts*, 2020, **22**, 792-801, DOI: 10.1039/C9EM00503J.
- 690 58 V. Ponsin, C. Torrentó, C. Lihl, M. Elsner and D. Hunkeler, Compound-specific chlorine isotope  
691 analysis of the herbicides atrazine, acetochlor and metolachlor, *Anal. Chem.*, 2019, **91**, 14290–  
692 14298, DOI: 10.1021/acs.analchem.9b02497.